Middle-East Journal of Scientific Research 14 (5): 673-682, 2013
ISSN 1990-9233

DOI: 10.5829/idosi.mejsr.2013.14.5.1899

On the Possibility of Self-Rotation in Sink Flow

[1]Jalal Mohammadi, [2]Hassan Karimi,
[1]Mohammad-Hossein Hamedi and [3]Abdolrahman Dadvand

[1]Faculty of Mechanical Engineering,
K.N. Toosi University of Technology, Tehran, Iran
[2]Faculty of Aerospace Engineering, K.N. Toosi University of Technology, Tehran, Iran
[3]School of Mechanical Engineering, Urmia University of Technology, Urmia, Iran

Abstract: This paper aims to study the possibility of self-rotation (i.e., swirl generation in the absence of external factors) in sink flow both experimentally and numerically. The present study is motivated by the fact that there is no consensus among the researchers about either the possibility or impossibility of this phenomenon. The differences in problem geometry, set up, velocity measurement technique, extend of measurement and the parameter measured may distinguish this work from the previous studies. In the experimental study, the circulation value is measured along various streamlines. The Reynolds number based on the drain flow rate was increased up to several times the so-called critical value determined in the previous studies. In the numerical investigation, the three-dimensional model of the problem is simulated using a pressure-based finite volume method. The results evidence good agreement between the simulations and experiments. It was observed that, the net value of circulation in the flow domain would not increase relative to its inlet value. This would imply that no self-rotation phenomenon would happen unless there are external factors. It is also concluded that the circulation can be attributed to the asymmetry in the radial velocity as well as to the circulation at the inlet boundary.

Key words: Self-rotation · Sink flow · Bathtub vortex · Swirling flow · Stability · Symmetry breaking

INTRODUCTION

The sink flow with swirl velocity is a well-known phenomenon. When water is drained from a tank through a small hole, it undergoes a translational motion toward the hole and a rotational movement [1]. In spite of its universality, the mechanism of such vortex generation has not been explained adequately. The main difficulties are due to many effective parameters involved and the sensitivity of the bathtub vortex to external factors [2].

The appearance of swirl in the sink flow and the formation of the bathtub vortex can result from many factors. These include small asymmetries in the flow inlet, asymmetric temperature distribution, asymmetric air motion over the water surface, asymmetry in the initial or boundary conditions, residual fluid motion in the vessel, vessel vibration and effect of the Coriolis force due to the Earth's rotation [3-5]. It may be noted that the latter effect is negligibly small if the diameter of the tank is smaller than six feet [4, 5]. The basic unanswered questions are "Will swirl appear in sink flow if all the external factors are eliminated and the tank size is chosen sufficiently small?" and "Will swirl appear if the speed of a swirl-free flow exceeds some threshold value?"

The appearance of swirl in the fluid flow without any external factors, namely self-rotation [6], have been observed in many natural systems such as the liquid flow inside Taylor cones [6], natural convection flow in a vertical circular cylinder [7], horizontally oscillating water in a cylindrical container [8] and an electrically driven flow of mercury in a cup [9].

Fundamentally, there have been several experimental and numerical studies to investigate the possibility of self-rotation phenomenon and the related instability in the sink flow. However, there is no consensus among the researchers about either the possibility or impossibility of this phenomenon. The experimental studies showed that the swirl would appear in an initially swirl-free sink flow as

Corresponding Author: Jalal Mohammadi, Faculty of Mechanical Engineering, K. N. Toosi University of Technology, Tehran, Iran.

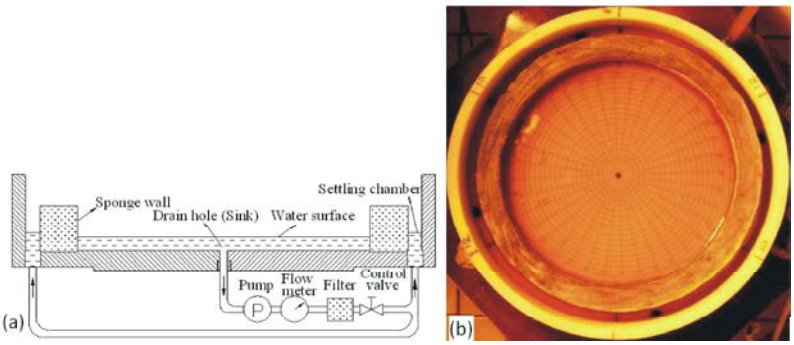

Fig. 1: (a) Geometry and nomenclatures of the experimental set-up and (b) Top view of the experimental tank.

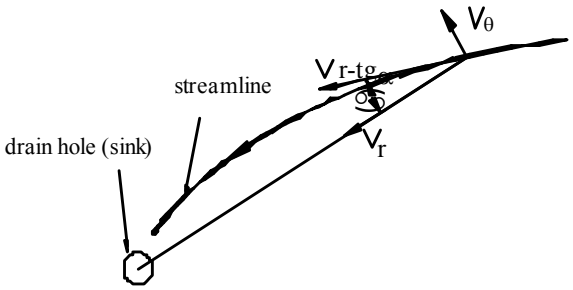

Fig. 2: Angle between the radial velocity vector and the streamline (α) and relation between the radial and azimuthal velocities ($V_\theta = V_r tg\alpha$).

the Reynolds number based on the sink flow rate increased above a critical value [10-12]. A linear stability of the boundary layer in sink flow was studied by Fernandez [13]. The instability was observed to occur at a relatively high Reynolds number where the flow becomes turbulent. While, the formation of the vortex in the sink was observed to happen at much lower Reynolds number. The sink flow stability was studied numerically based on the axisymmetric and three-dimensional (3D) models by [12, 14, 15]. It was observed in [14, 15] that the flow is stable and no swirl is generated for all the Reynolds (Re) numbers tested. De Felice [12] found no swirl in the axisymmetric model. In 3D model however, both instability and swirl generation were observed for the Re numbers above a critical value. In fact, one can see different and conflicting findings from the existing studies, i.e., some researchers accept the existence of self-rotation in the sink flow and some not. On the other hand, it is deduced from these studies that the circulation generation contradicts the conservation of angular momentum [2]. Therefore, this problem needs to be studied and characterized in more detail.

Note that in the present work, self-rotation is regarded either as the spontaneous appearance of swirl in an initially swirl-free flow (swirl generation) or as the increase of circulation with respect to its inlet value (circulation generation). In both cases, the circulation value increases. Note that, the increase of the swirl (azimuthal) velocity by decreasing the radius with constant circulation as it occurs in converging flows is not related to self-rotation. This strong growth of local azimuthal velocity near the bathtub drain hole can be explained by Lord Kelvin's circulation theorem. This theorem stating the conservation of circulation is a hydrodynamic version of a more general principle: the conservation of angular momentum [16].

In the present work, the possibility of circulation generation in the 3D sink flow is studied both experimentally and numerically. We simulate the sink flow or the bathtub vortex on a cylindrical tank with a central drainpipe and a free surface (Figure 1). In the experiments, we have attempted to construct a set-up with minimum possible inlet asymmetry and examined the circulation evolution along various streamlines. Although recently suggested by Bøhling *et al*. [17], such a set-up has not been constructed thus far. The flow instability in the azimuthal direction as well as the sharp changes in the circulation is examined as the drain flow rate is increased. Some different and advantageous aspects distinguish the present experiments from the previous ones. Unlike the previous experiments, we have employed a new velocity measurement technique, which imposes no limitation on the experimental arrangement. In addition, it can measure the velocity at any point and along various streamlines in the fluid domain. It is noted that the velocity measurements in the previous works were restricted to a point in the flow [10], along a line [11] or to the free surface close to the drain hole [12], which may lead to imprecise results and interpretations. In the numerical study, the three-dimensional model of the experiment (Figure 3) is simulated and the effect of boundary condition asymmetry on the circulation is studied.

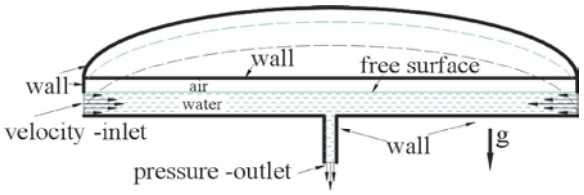

Fig. 3: Geometry and nomenclatures of the 3D numerical domain (half part has been shown) with the same dimensions as the experimental setup; g is the acceleration of gravity.

The rest of the paper is organized as follows: In Section 2, the experimental set-up as well as the method of velocity measurement is briefly described. Section 3 contains the governing equations of motion and the numerical procedure. In Section 4, the experimental and numerical results are presented and discussed. In Section 5, we summarize the main findings and present the conclusions. Finally, in the appendix the error analysis of the experimental results is given.

MATERIALS AND MATHODS

Experimental Set up: The experimental setup is sketched in Figure 1a. The open-top cylindrical tank of 300 mm diameter and 70 mm height is filled with the working fluid up to 10 mm height. The tank is made of polyamide and is divided into two main parts: the central part surrounded by a sponge and the lateral part located between the tank inner wall and the sponge (i.e., settling chamber). The sponge is used to suppress the flow disturbances, which may be induced in the settling chamber by the feed pump. The working fluid (water) is drained at a volume rate of Q through a circular drain hole of 5 mm diameter, which is located at the bottom (center) of the tank and then is returned to the tank through four holes in the settling chamber. The water is circulated by a pump and the flow rate is adjusted by turning a stopcock. The flow rate is measured using a flow meter with an uncertainty of about 1 Lit/hr while the temperature is measured with a thermocouple with an uncertainty of about 0.1°C. The temperature is used to calculate the kinematic viscosity ν of water.

Velocity Measurement: The thymol blue technique was used for velocity measurement. The working fluid is prepared by solving 0.04% per weight of thymol blue in distilled water. The solution was then titrated, by adding NaOH drop, just to the acid side of the endpoint of the indicator (pH≈8.0) so that the solution was orange yellow [18]. Two electrodes were introduced into the fluid, namely, a cathode and an anode. The cathode was a thin wire (0.1 mm in diameter) placed perpendicular to the mean flow direction at the upstream of the flow (i.e., at the central part near the inner wall of the sponge). The anode comprised two thick wires and it was placed at the settling chamber. A direct current (dc) voltage of 36V was applied for 1.5s, by automatic electric key, to produce the dye. A thin line of dark blue was marked around the cathode. It was deformed by the local velocity, as it was moving with the flow (Figure 4). Note that this labeling method does not introduce any change of density. We also found that illuminating with sodium-yellow light would improve the contrast significantly because the parent solution is orange yellow and the dye is blue. Hence, the dye looked black in the illumination, with a bright background. A full HD digital video camera capable of obtaining images at a frame rate of 60 fps was utilized to record, from the top view, the evolution of the marked fluid line.

The radial velocity V^*_r is obtained by measuring the time it takes for the tip of the marked fluid parcel to travel a given radial distance. It should be mentioned that the values of V^*_r and $V^*_{r-\theta}$ parameters are very close to each other according to the relation $V^*_r = V^*_{r-\theta} \cos\alpha$, where α is the angle between the direction of the radial component of the velocity vector and the corresponding streamline (Figure 2). In the experiments carried out in the present work, the maximum value of α is found to be about 0.14 radian. Therefore, the difference between these two parameters is at most 1 percent.

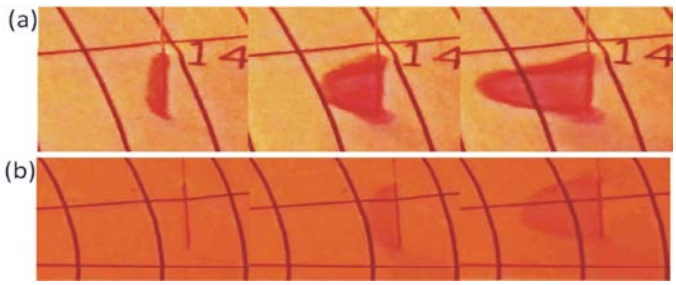

Fig. 4: Side view of dye production around the cathode wire at different distances from the drainpipe: (a) r^* = 93mm, (b) r^* = 47mm.

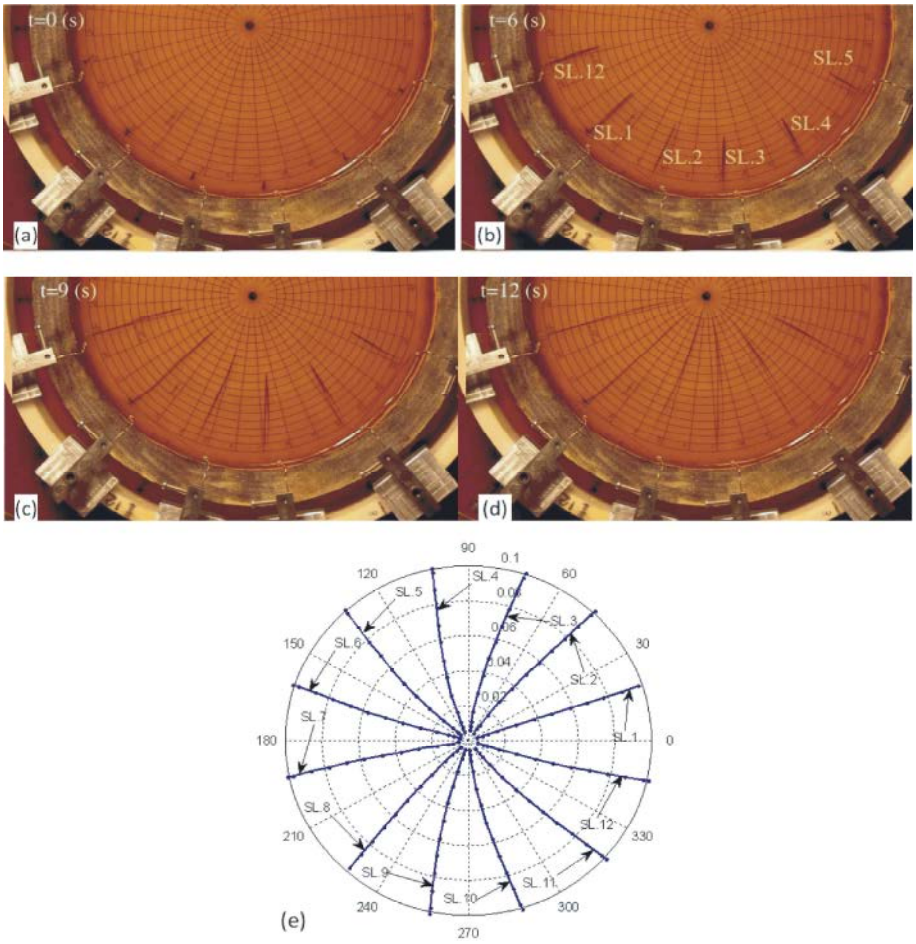

Fig. 5: Sequential images (frames a-d) of top view of the dye motion along the streamlines 1-5 and 12 at the times (in seconds) 0, 6, 9 and 12. (e) Streamlines 1 to 12 in the r-θ plane; the direction of the azimuthal velocity is positive for streamlines 1-6 and negative for streamline 7-12.

According to Figure 2, the azimuthal velocity can be obtained from the following relation,

$$V_\theta^* = V_r^* tg\alpha \quad (1)$$

where, V^*_r and V^*_θ are the magnitudes of the radial and azimuthal velocity components, respectively. The value of α can be obtained by knowing the path equation of the tip of the color bulk (i.e. streamline). To extract this path equation, the different frames of color bulk motion were entered into AutoCAD software and the coordinates of the tip of the color bulk were determined. Consequently, the path equation was obtained by fitting a function to these points. The streamlines 1-12 are shown in Figure 5e.

The circulation Γ^* along the streamline can be calculated from the following relation,

$$\Gamma^* = r^* V_\theta^*$$

$$\Gamma^* = r^* V_r^* tg\alpha \quad (2)$$

Numerical Study: In the numerical simulations, the 3D model of the experiment is simulated using direct numerical simulation (DNS), where the full Navier-Stokes equations are solved without any turbulence model introduced. The influence of asymmetry at the inlet boundary on the circulation is examined.

Governing Equations: We consider the flow inside the cylindrical container as sketched in Figure 3. Water with a flow rate Q enters the cylindrical tank horizontally through the circular side. A small drainpipe of diameter (d) draws the fluid out of the container from the center of the bottom wall. The flow in the cylindrical tank is assumed laminar, steady and incompressible. We denote the radius of the tank R, the depth of the free surface H and the length of the drainpipe L_p.

The volume of fluid (VOF) model is applied for modeling the free surface flow and two-phase flow (water and air). The tracking of the interface between the phases is accomplished by solution of a volume fraction continuity equation for one of the phases (here, water), as given in Eq. (3). Air volume fraction is computed using the constraint shown in Eq. (4),

$$\vec{V} \cdot \nabla \varepsilon_w = 0 \tag{3}$$

$$\varepsilon_w + \varepsilon_a = 1 \tag{4}$$

Here ε_w and ε_a are the volume factions of water and air, respectively.

The viscosity μ and density ρ within each computational cell are determined based on the weighted average volume fraction, as shown in Eqs. (5) and (6),

$$\rho = \varepsilon_w \rho_w + (1-\varepsilon_w)\rho_a \tag{5}$$

$$\mu = \varepsilon_w \mu_w + (1-\varepsilon_w)\mu_a \tag{6}$$

A single set of continuity equation and momentum equations for two fluids as shown in Eqs. (7)-(10) is solved throughout the domain. We use the cylindrical polar coordinates (r, θ, z), with velocity field (V_r, V_θ, V_z), such that the z-axis is chosen as the axis of the cylinder and the bottom wall of the container lies on the plane z=0. In order to normalize the governing equations, the drainpipe diameter d and the average flow velocity $4Q/(\pi d^2)$ through it are considered as the length and velocity scale factors, respectively. Therefore, the dimensionless form of the governing equations are written as follows,

$$\frac{1}{r}\frac{\partial}{\partial r}(rV_r) + \frac{1}{r}\frac{\partial}{\partial \theta}(V_\theta) + \frac{\partial}{\partial z}(V_z) = 0 \tag{7}$$

$$(V.\nabla)V_r - \frac{V_\theta^2}{r} = -\frac{\partial P}{\partial r} + \frac{1}{\mathrm{Re}}(\nabla^2 V_r - \frac{V_r}{r^2} - \frac{2}{r^2}\frac{\partial V_\theta}{\partial \theta}) \tag{8}$$

$$(V.\nabla)V_\theta + \frac{V_r V_\theta}{r} = -\frac{1}{r}\frac{\partial P}{\partial \theta} + \frac{1}{\mathrm{Re}}(\nabla^2 V_\theta + \frac{2}{r^2}\frac{\partial V_r}{\partial \theta} - \frac{V_\theta}{r^2}) \tag{9}$$

$$(V.\nabla)V_z = -\frac{\partial P}{\partial z} + \frac{1}{Fr} + \frac{1}{\mathrm{Re}}(\nabla^2 V_z) \tag{10}$$

where, $Fr = \frac{16Q^2}{\pi^2 d^5 g}$, $\mathrm{Re} = \frac{4Q}{\pi d \upsilon}$.

In the present work, we seek the circulation (i.e., angular momentum per unit mass) defined as $\Gamma = rV_\theta$ and $G^* = r^* V_\theta^*$ in dimensionless and dimensional forms, respectively.

At the container inlet (Figure 3), the axial velocity is zero and we assume a parabolic profile for the radial and the azimuthal velocities:

$$V_r(\theta,z) = \bar{V}_r(\theta)_{in} 1.5(-z^2 + 2z), \quad r = 20, \quad 0 < z < 2$$

$$V_\theta(\theta,z) = \bar{V}_\theta(\theta)_{in} 1.5(-z^2 + 2z), \quad r = 20, \quad 0 < z < 2 \tag{11}$$

$$V_z = 0$$

Such assumptions will match the experimental boundary conditions at both the bottom wall and the free surface. Here $\bar{V}_r(\theta)_{in}$ and $\bar{V}_\theta(\theta)_{in}$ are respectively the average values of V_r and V_θ at the inlet obtained from the experiments. At the solid walls (Figure 3), all the velocities vanish, i.e. at these boundaries we can write,

$$V_r = 0, \quad V_\theta = 0, \quad V_z = 0 \tag{12}$$

At the exit of the drainpipe, the pressure outlet boundary condition is chosen.

Computational Approach: A finite volume discretization approach has been employed to solve the governing Eqs. (3)-(10) subject to the boundary conditions Eqs. (11) and (12). The SIMPLE iterative algorithm is used to solve the pressure-correction equation [19] and the second-order upwind difference scheme is used for discretization of the convection terms. An unstructured grid has been used. It is found that a grid with 528,000 hexahedral cells can produce the grid independent solution.

RESULTS AND DISCUSSIONS

The experimental results are associated with Re=4250 where the drain flow rate Q, the drainpipe diameter d and the kinematic viscosity *v* are set to be 60 l/h, 5mm and 1e – 6m^2/s, respectively. Note that the current drain flow rate Q is about 1.7 times the so-called critical value obtained in [10]. In addition, the Re number considered in the present

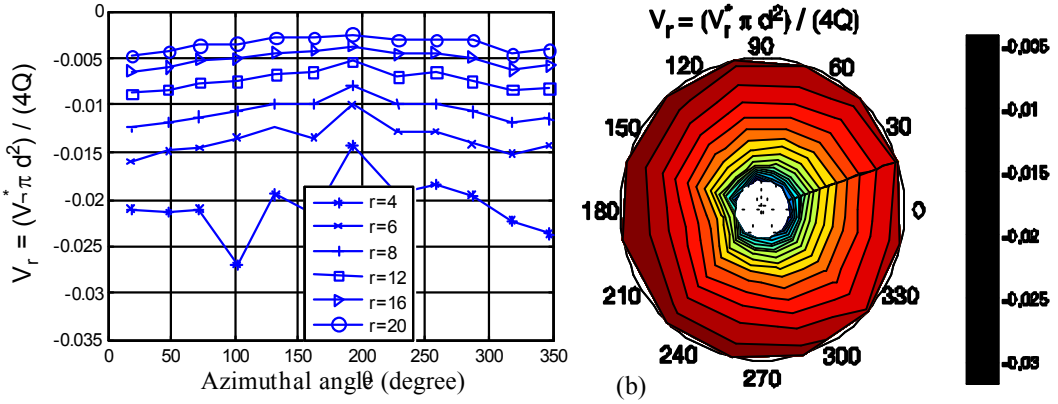

Fig. 6: (a) Experimental results of dimensionless radial velocity V_r variations versus azimuthal angle θ measured at various dimensionless radii r, (b) contour of V_r in the r-θ plane. It is clear that, the radial velocity is not azimuthally symmetric.

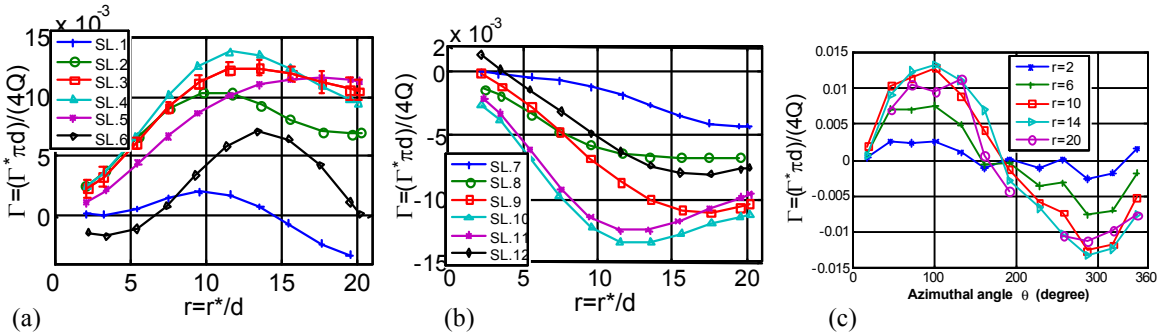

Fig. 7: Radial variations of dimensionless circulation Γ along streamlines 1-6 (a) and streamlines 7-12 (b). The measurement error range is shown at streamline 3. We see positive circulation values at streamline 1-6 and negative values at streamline 7-12. (c) Azimuthal profile of dimensionless circulation Γ at various radii. The maximum absolute value of normalized circulation occurs at r~12.

work is about 3.1 and 9.5 times the critical values tested in [11] and [12], respectively. Later we show that even at this high Re number no self-rotation will be observed.

The sequential images of dye motion are shown in Figure 4 from the side view. It can be observed that radial velocity has zero value on the tank floor, the maximum value in the middle of water depth and negligible value at the free surface.

Figure 5 demonstrates the direction of the dye motion along the streamlines 1-5 and 12 at times (in seconds) 0, 6, 9 and 12. The time t = 0 corresponds to the moment the tip of color bulk reaches the radius of 100 mm. It is observed that both the radial and azimuthal velocities vary from one streamline to another. At a given instant, the distance traversed by the color bulk tip is different from a streamline to another implying different radial velocities for different streamlines so that it will increase from the streamline 5 to the streamline 1. Moreover, the direction of the azimuthal velocity V_θ can be deduced from the direction of the color bulk motion relative to the radial lines of the scaled plane on the tank floor. For instance, the direction of V_θ is positive for streamlines 1 to 5, if counterclockwise is defined positive.

The radial velocity associated with different streamlines has been depicted in Figure 6. It can be seen that the radial velocity increases as r decreases, which is due to the conservation of mass (i.e., the continuity). The radial velocity is found to be a continuous smooth function of θ as $V_r(\theta) = a + b\sin(\theta/2)$. In addition, the maximum and minimum absolute values of V_r correspond to the streamlines 1 (θ~20) and 7 (θ~190), respectively. Furthermore, for large radii the radial velocity changes smoothly in the azimuthal direction. However, it will become irregular at small radii, because the measurement error will increase as the radius decreases.

The circulation evolution along streamlines 1-12 is presented in Figure 7 showing that, along almost all of the streamlines the absolute value of circulation increases from inlet (r=20) to r=12 and decreases thereafter towards the drainpipe such that it approaches zero very close to

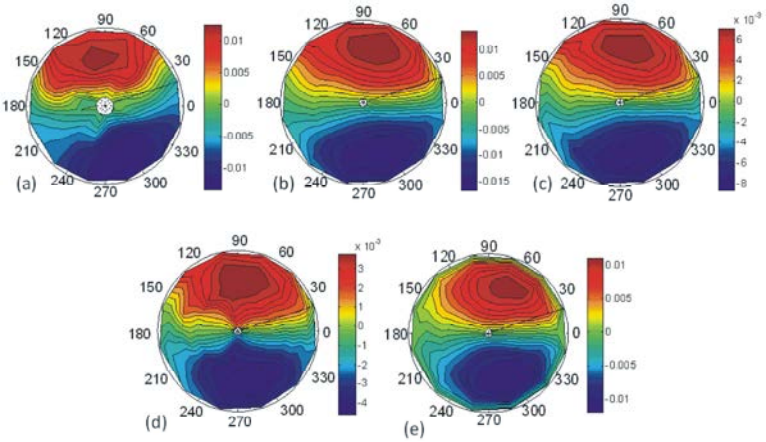

Fig. 8: Dimensionless circulation Γ in the r-θ plane: (a) experimental result extracted from Fig. 7; (b-e) numerical results; (b) numerical results under the same conditions as the experiment; (c) and (d) numerical results under the same conditions as the experiment except that the asymmetry of the radial velocity as well as the circulation value at the inlet have been reduced to one-half and one-fourth of the experiment, respectively. (e) numerical results under the same condition as the experiment except the circulation value at the inlet is chosen zero.

the drainpipe. It is observed that the value of circulation varies in the θ direction in accordance with the function $\Gamma(\theta) = A\sin\theta$, where A is a constant. The maximum and the minimum values of the dimensionless circulation Γ are equal to 0.0135 and -0.0134 pertaining to the streamlines 4 (θ~105) and 10 (θ~290), respectively. It is worth noting that the sign of the circulation is positive for the streamlines 1-6 (i.e., θ = θ° to 180°) and is negative for the streamlines 7-12 (i.e., θ = 180° to 360°). As we shall see from numerical results, this may originate from the inlet radial velocity that is not fully symmetric, because even a small misalignment at the inlet can introduce asymmetries in the radial velocity. Under such circumstances, the fluid particles would move from the points with larger inlet radial velocity towards the points with smaller inlet radial velocity, leading to the formation of positive and negative circulations in the flow. On the other hand, throughout the domain, the net value of circulation is just about zero and it will not increase relative to its net value at the inlet. This implies that no circulation is generated and hence, there is no self-rotation in the sink flow.

In order to substantiate the accuracy of the numerical results, the boundary conditions as well as the streamlines are chosen to be the same as those of the experiment. The contours of numerical result of circulation along the streamlines in the r-θ plane are shown in Figure 8b. This result is comparable with the results in Figure 8a obtained based on the experimental values of circulation shown in Figure 7. The results evidence good agreement between the simulation and experiment. In addition, although the maximum and minimum values of the numerical circulation are almost the same as those of the experiment, their occurrence locations are slightly different. This may be attributed to the inherent laboratory measurement errors, non-smoothness and/or non-flatness of the bottom wall of the tank and slant of the experimental setup.

In order to examine the effect of inlet asymmetry, the asymmetry of the inlet radial velocities $(V_r(\theta) - \overline{V}_r)$ as well as the inlet circulation values Γ(θ) have been reduced to one-half and one-fourth of their experimental counterpart and shown respectively in Figures 8c and 8d. It can be seen that throughout the domain, the circulation values have been decreased to one-half and one-fourth of the experimental ones as well. This reveals that the origin of the circulation in the sink flow may be attributed to the asymmetry in the inlet radial velocity and non-zero value of circulation at inlet. Therefore, the circulation in the sink flow can be fully removed by removing these external factors at the flow inlet. This would confirm that the generation of circulation in the sink flow is not spontaneous.

Another numerical example is performed under the same condition as the experiment except that the circulation value at the inlet is set equal to zero (i.e., Γ=0). The circulation value along the streamlines in the r-θ plane for this case is shown in Figure 8e, which is almost the same as its counterpart shown in Figure 8a. It is found from comparing this figure with Figure 8a, 8c and 8d that, the circulation generated in the fluid domain is mainly due to asymmetry in the radial velocity rather than the non-zero circulation at the inlet.

The self-generation of swirl in the sink flow for the Re numbers above some critical value was claimed to happen by few researchers ([10-12, 14], for examples). This idea can be rebutted for the following reasons: The results in [10-12, 14] were based on the variations in the value of azimuthal velocity V_θ, instead of being based on the circulation Γ. This could lead to misinterpretation of the results because V_θ experience high variations compared to Γ in the flow field. In addition, in the previous studies, the swirl was measured at some limited locations in the flow field, which might lead to misunderstanding of the results due to the meagerness of the data needed. Furthermore, some researchers refuted the self-rotation in the sink flow (see [13,15], for examples) simply because they did not observe the phenomenon. Finally, self-rotation phenomenon in the sink flow is in contradiction with the conservation of angular momentum principle [2].

CONCLUSIONS

This study aims to investigate the possibility of circulation generation in the absence of external factors (i.e., self-rotation) in the sink flow both experimentally and numerically. In the experiment, the circulation evolution along various streamlines is studied, where both the drain flow rate and the ensuing Reynolds number are chosen several times higher than the so-called critical ones. The inlet has been designed in order to minimize any introduced angular momentum. The results revealed that the net value of circulation would not increase relative to the net inlet value implying that in the absence of external factors no self-rotation happens in the sink flow. The numerical simulation of the problem has been carried out using the same geometry and boundary conditions as the experiment. There are good agreements between the numerical and experimental results. The positive and negative values of circulation observed in the flow domain originate mainly from the asymmetries in the radial velocity and non-zero value of circulation at the inlet. The circulation in the domain can be fully removed by designing the inlet in such way that these factors could be eliminated. This confirms once again that there would be no spontaneous generation of circulation in the sink flow.

Appendix

Error Analysis of the Experimental Results: In this appendix, we study the accuracy of the experimental results presented in the current paper. For this purpose, the measured parameters and the corresponding error range associated with the streamline 3, for instance, are presented. The radial velocity and the corresponding error range for streamline 3 is shown in Figure 9a. The following two errors may be inevitable: error in determining the time it takes for the tip of the color bulk to traverse a certain radial distance and error in estimating the instant velocity from the mean velocity. These two errors increase as the radius decreases (Figure 9a).

The streamline coordinates could be determined with an error of 0.025-0.040 mm using AutoCAD, leading to an uncertainty of 0.0035-0.0070 radian in α as shown in figure 9b. The error, which arises when evaluating Γ^* can be interpreted by knowing that Γ^* depends on V_r^* and α according to Eq.(2). The error range and value of Γ^* for the streamline 3 are depicted in figure 9c.

In addition to the above-mentioned errors, there are other two errors, which can affect the accuracy of the experimental results. These errors can be due to the difference in the reflective index of water and air and non-perpendicular placement of camera relative to the water surface. They depend on the distance of the camera from the water surface. In the experiments, we tried to minimize these errors by placing the camera at a distance of 2000 mm from the water surface. The errors that arise due to these two factors when specifying the streamline coordinates are estimated to be less than 0.1% and 0.2%, respectively which are much less than the error values mentioned in the previous paragraph.

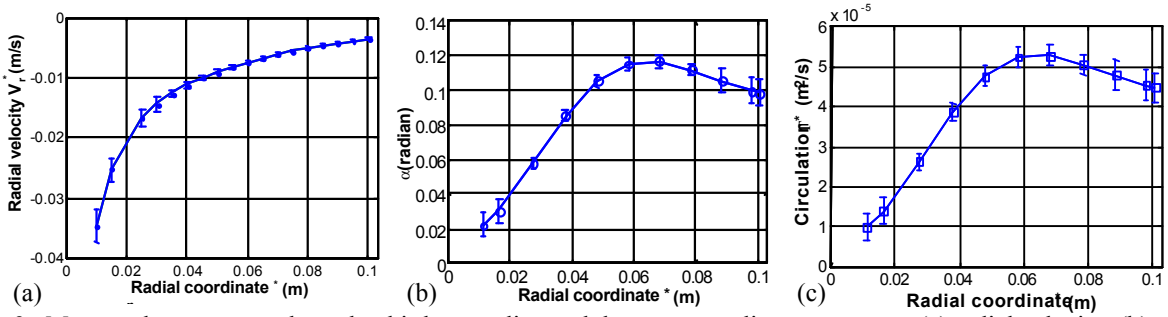

Fig. 9: Measured parameters along the third streamline and the corresponding error range: (a) radial velocity; (b) angle α between the radial velocity vector and the corresponding streamline; (c) circulation.

Introducing the cathode wire into the fluid flow may add another error to the experimental results. Based on the laminar wake theory, the labeled fluid velocity can reach the free stream velocity in a downstream distance of approximately 70 diameters of wire [18]. Therefore, for eliminating the influence of the introduced cathode wire on the experimental results, our measurements were carried out at a distance more than 70 diameters behind the wire.

Nomenclature:

d Drainpipe diameter (m)
Fr Froude number, $Fr = 16Q^2/(p\, d^5 g)$
g Gravitational acceleration (ms^{-2})
H Height of the free surface (m)
P Dimensionless pressure, $P=P^*\pi^2d^4/(16\rho Q^2)$
Q Volumetric drain flow rate (m^3s^{-1})
R Radius of the tank (m)
r^* Radial coordinate (m)
r Dimensionless radial coordinate, $r = r^*/d$
Re Reynolds number, $Re = 4Q/(\pi d\upsilon)$
V^*_r Radial velocity (ms^{-1})
V^*_θ Azimuthal velocity (ms^{-1})
V_z^* Axial velocity (ms^{-1})
$V^*_{r-\theta}$ Velocity in the r – θ Plane (ms^{-1})
V_r Dimensionless radial velocity, $v_r = \frac{v_r^* \pi d^2}{4Q}$
V_θ Dimensionless azimuthal velocity, $v_\theta = \frac{v_r^* \pi d^2}{4Q}$
V_z Dimensionless axial velocity, $v_z = \frac{v_z^* \pi d^2}{4Q}$
z^* Axial coordinate (m)
z Dimensionless axial coordinate, $z = z^*/d$

Greek Symbols:

υ Kinematic viscosity (m^2s^{-1})
μ Dynamic viscosity (Pa s)
ρ Density ($kg.m^{-3}$)
ε Volume faction
α The angle between the radial velocity vector and the corresponding streamline (radian)
Γ^* Circulation i.e. angular momentum per unit mass (m^2s^{-1})
Γ Dimensionless circulation, $\Gamma = \frac{\Gamma^* \pi d}{4Q}$

Subscripts:

w Water
a Air

REFERENCE

1. Klimenko, A.Y., 2001. Moderately strong vorticity in a bathtub-type flow. Theoretical and Computational Fluid Dynamics, 14(4): 243-257.
2. Vladimir, S. and H. Fazle, 1999. Collapse, symmetry breaking and hysteresis in swirling flows. Annual Review of Fluid Mechanics, 31: 537-566.
3. Lugt, H.J., 1983. Vortex Flow in Nature and Technology. John Wiley & Sons.
4. Shapiro, A.H., 1962. Bath-tub vortex. Nature, 196: 1080-1081.
5. Trefethen, L.M., R.W. Bilger, P.T. Fink, R.E. Luxton and R.I. Tanner, 1965. The bath-tub vortex in the southern hemisphere. Nature, 207: 1084-1085.
6. Herrada, M.A. and A. Barrero, 2002. Self-rotation in electrocapillary flows. Physical Review E, 66(3): 036311-036320.
7. Torrance, K.E., 1979. Natural convection in thermally stratified enclosures with localized heating from below. Journal of Fluid Mechanics, 95(3): 477-495.
8. Funakoshi, M. and S. Inoue, 1988. Surface waves due to resonant horizontal oscillation. Journal of Fluid Mechanics, 192: 219-247.
9. Bojarevics, V., Y.A. Freibergs, E.I. Shilova and E.V. Shcherbinin, 1989. Electrically Induced Vortical Flows. Kluver Academic.
10. Kawakubo, T., Y. Tsuchiya, M. Sugaya and K. Matsumura, 1978. Formation of a vortex around a sink: a kind of phase transition in a nonequilibrium open system. Physics Letters A, 68(1): 65-66.
11. Fernandez-Feria, R. and E. Sanmiguel-Rojas, 2000. On the appearance of swirl in a confined sink flow. Physics of Fluids, 12(11): 3082-3085.
12. De Felice, V.F., 2008. Il vortice a superficie libera in quanto instabilità (The free surface vortex due to instability). Ph.D. thesis, degli Studi di Salerno University.
13. Fernandez-Feria, R., 2002. Stability analysis of boundary layer flow due to the presence of a small hole on a surface. Physical Review E, 65: 036307.
14. Sanmiguel-Rojas, E., 2002. Sobre el fenómeno de la autorrotación (On the phenomenon of self-rotation), Ph.D. thesis, Malaga University.
15. Sanmiguel-Rojas, E. and R. Fernandez-Feria, 2006. Nonlinear instabilities in a vertical pipe flow discharging from a cylindrical container. Physics of Fluids, 18(2): 024101.

16. Tyvand, P.A. and K.B. Haugen, 2005. An impulsive bathtub vortex. Physics of Fluids, 17(6): 062105.
17. Bøhling, L., A. Andersen and D. Fabre, 2010. Structure of a steady drain-hole vortex in a viscous fluid. Journal of Fluid Mechanics, 656: 177-188.
18. Merzkirch, W., 1987. Flow Visualization. Academic Press.
19. Norzieha M., K.M. Prashanta, R.J. Peter and A. Norsarahaida, 2010. A numerical simulation of unsteady blood flow through multi-irregular arterial stenoses. Applied Mathematical Modelling, 34(6): 1559-1573.